PAPER

Modeling the strain rate-, hold time-, and temperature-dependent cyclic behaviors of amorphous shape memory polymers

IOP Publishing Smart Materials and Structures
Smart Mater. Struct. **27** (2018) 075050 (10pp) https://doi.org/10.1088/1361-665X/aaca50

Modeling the strain rate-, hold time-, and temperature-dependent cyclic behaviors of amorphous shape memory polymers

Hao Zeng[1], **Jinsong Leng**[2,4], **Jianping Gu**[3], **Chenxi Yin**[1] and **Huiyu Sun**[1,4]

[1] State Key Laboratory of Mechanics and Control of Mechanical Structures, Nanjing University of Aeronautics and Astronautics, 29 Yudao Street, Nanjing 210016, People's Republic of China
[2] Center for Composite Materials and Structures, Harbin Institute of Technology, Harbin 150080, People's Republic of China
[3] Jiangsu Key Laboratory of Advanced Structural Materials and Application Technology, School of Materials Science and Engineering, Nanjing Institute of Technology, Nanjing 211167, People's Republic of China

E-mail: hysun@nuaa.edu.cn and lengjs@hit.edu.cn

Received 2 February 2018, revised 7 May 2018
Accepted for publication 5 June 2018
Published 22 June 2018

Abstract

This paper presents intensive studies on the strain rate-, hold time-, and temperature-dependent cyclic behaviors of amorphous shape memory polymers (SMPs). The cyclic characteristics play a vital role in the application of SMPs since the materials suffer cyclic loadings commonly in engineering. A multi-branch fractional derivative model is employed in the paper to investigate the complicated mechanisms underlying the cyclic behaviors. And a modified Eying model is incorporated with the fractional derivative model to describe the temperature-dependent yielding and post-yielding behaviors. A rate-dependent yielding factor is proposed in the study to depict the influence of strain rates. The validity and adaptability of the model are verified through comparisons between the simulations and experimental results of two different materials subjected to different loading conditions. In addition, detailed parameter studies provide effective suggestions on improving the performance of SMPs under various conditions.

Keywords: shape memory polymers, cyclic tension behaviors, fractional derivative model, rate-dependent yielding factor

(Some figures may appear in colour only in the online journal)

1. Introduction

In the last decades, shape memory polymers (SMPs) have gained much attention for its ability to remember one or several permanent shapes, and recover to them from a temporary shape once some appropriate stimuli such as temperature [1, 2], light [3, 4], or magnetic field [5, 6], are imposed. Due to their promising applications in biomedical devices [7] and aerospace structures [8], the thermomechanical behaviors of SMPs especially thermal-induced SMPs and their composites have been extensively investigated.

In general, there are two kinds of constitutive theories for thermal-induced SMPs: thermoviscoelastic models and phase transition models. The first thermoviscoelastic model was proposed by Tobushi *et al* [9, 10] in 1996 by introducing a nonlinear slip element to a three-element Maxwell model. Researchers have developed many effective models based on this theory [11–15]. For example, Diani *et al* [16] employed the generalized Maxwell model to simulate the viscoelastic behavior of amorphous SMPs, and the simulation results in a commercial finite element software of the developed model agreed well with the experimental shape memory thermomechanical torsion data even in a large deformation regime. The theory was then applied to model the thermomechanical

[4] Authors to whom any correspondence should be addressed.

properties of fiber reinforced SMP composites by Al Azzawi *et al* [17] in 2017. Details of implementation in ABAQUS were given in the paper and the results of different fiber content all showed good agreement with the experimental results. A much more effective thermoviscoelastic constitutive model was proposed by Xiao *et al* [18], which incorporates several time- and temperature-dependent mechanisms including viscoelasticity, multiple structure relaxation, multiple stress relaxation and stress-activated viscoplastic flow. The models are able to well describe the thermal-induced nonlinear shape memory effects (SMEs) and viscoplatic behaviors in the glassy region but are relatively complicated. On the other side, the phase transition model for SMPs was firstly proposed by Liu *et al* [19] in 2006, in which a switchable phase is hypothesized to spread evenly in the materials and switch from the rubbery state at high temperatures to the glassy state while the temperature decreases. This approach also drew considerable attention [20–24] due to its briefness in understanding the SMEs. Li *et al* [25] combined the advantages of phase transition models and viscoelastic models, and developed a phase transition-based viscoelastic model to predict the SMEs. However, the so-called phase is phenomenological in amorphous SMPs and the transformation rule of the phase is also difficult to well describe.

While many constitutive models were developed to study the thermomechanical behaviors such as thermomechanical cycle behaviors, uniaxial tension or compression behaviors and cold deformation behaviors of SMPs, less attention has been paid to their performance when the materials are subjected to cyclic loading conditions. The materials usually suffer cyclic loadings in engineering, and their cyclic characteristics determine the service life of the specific devices. So it is very important to investigate the cyclic behaviors under various conditions. Yu *et al* [26] utilized a multi-branch linear Maxwell model to predict the mechanical response of the Veriflex-Epoxy thermosetting SMPs under cyclic tension at high temperatures above the glass transition region. The model is able to well describe the ratchet behaviors and the strain rate-, hold time- and temperature-dependent cyclic behaviors of the material at high temperatures but is incapable at temperatures below or around the glass transition region. And Pieczyska *et al* [27] employed a phase transition model to study the yielding phenomenon of the polyurethane SMPs subjected to cyclic tension at low temperatures below the glass transition region. Though the imposed deformation is small (0.6%), the model is unable to well describe the ratchet behaviors. In addition, the temperature variation is so small that it is not necessary to consider phase transition in the cyclic tension experiments.

In the paper, the fractional derivative theory is utilized to describe the linear temperature-dependent thermoviscoelastic behaviors of SMPs. The fractional model is much concise compared to the nonlinear thermoviscoelastic or phase transition models, and reduces a lot of parameters compared to the linear Maxwell model [28]. But the conventional fractional models are unable to describe the yielding and post-yielding behaviors below the glass transition region. To settle this issue, we incorporate the Eying model to describe the temperature-dependent stress-activated viscoplastic properties of SMPs. In addition, the experimental results show that the strain rate also influences the yielding behavior, which has rarely been considered in existing models. A rate-dependent yielding factor is proposed in the paper, by which the Eying model is modified to capture the strain rate-dependent yielding behaviors of the SMPs. The comparisons between the simulations and the experiments of two different materials under different loading conditions validate the present model. Then detailed parameter studies are carried out to investigate the influences of some factors such as temperature, strain rate, loading cycle and hold time on the cyclic performance of the materials. The residual strain ratio is defined to quantitatively characterize the cyclic performance. Many helpful and interesting results are obtained in the last section.

2. Constitutive model

2.1. Kinematics

Figure 1 shows the multi-branch fractional Maxwell model in which the 'spring-pot' element replaces the conventional dash-pot [29]. Correspondingly, the constitutive relation of this element is

$$\sigma(t) = E^{1-\alpha}\eta^{\alpha}D^{\alpha}\varepsilon(t) = E\tau^{\alpha}D^{\alpha}\varepsilon(t), \tag{1}$$

where E, η and $\tau = \eta/E$ are the Young's modulus, viscosity and relaxation time, respectively, α is the fractional derivative parameter, and D^a represents fractional derivative i.e.

$$D^{\alpha}f(t) = DD^{\alpha-1}f(t), \tag{2}$$

where D denotes differentiation and the operation $D^{\alpha-1}$ can be obtained by the Riemann–Louiville fractional integral

$$D^{\alpha-1}f(t) = \int_0^t \frac{(t-\tau)^{-\alpha}}{\Gamma(1-\beta)} f(\tau)\mathrm{d}\tau, \tag{3}$$

where Γ is the gamma function. And it should be noted that the fractional derivative parameter α is limited to $0 \leqslant \alpha \leqslant 1$, and the specific 'spring-pot' turns into a simple spring as $\alpha = 0$ and a dash-pot as $\alpha = 1$.

As shown in figure 1, the E_0 branch represents the equilibrium behavior of the materials. And viscoelastic behaviors are described by the n non-equilibrium branches, in which E_i is the modulus of the spring and the specific spring-pot element is represented by $E_i\tau_i{}^{\alpha_i}$. Similar to the conventional generalized Maxwell model, the constitutive relation of the multi-branch fractional Maxwell model can be deduced as follows. The stress–strain relationship of the ith branch is got

$$\sigma_i = E_i\varepsilon_i^e = E_i\tau_i^{q_i}D^{\alpha_i}\varepsilon_i^v, \tag{4}$$

where ε_i^e and ε_i^v are the elastic and viscous strain respectively, and $\varepsilon_i^e + \varepsilon_i^v = \varepsilon_i$. Taking the Laplace transform of equation (4) and then eliminating the corresponding $\overline{\varepsilon}_i^e$ and $\overline{\varepsilon}_i^v$, we have

$$(1 + \tau_i^{\alpha_i}s^{\alpha_i})\overline{\sigma}_i = E_i\tau_i^{\alpha_i}s^{\alpha_i}\overline{\varepsilon}_i. \tag{5}$$

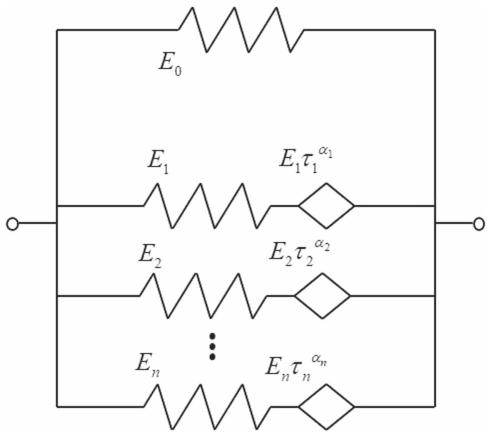

Figure 1. Illustration of the multi-branch fractional Maxwell model.

Accumulating the $n + 1$ branches and then applying the inverse Laplace transform, one can obtain the final form of the constitutive equation of the multi-branch fractional Maxwell model as

$$\sigma = \left(E_0 + \sum_{i=1}^{n} \frac{E_i \tau_i^{\alpha_i} D^{\alpha_i}}{1 + \tau_i^{\alpha_i} D^{\alpha_i}}\right)\varepsilon. \tag{6}$$

Generally speaking, it is still complicated to describe the thermoviscoelastic behavior by equation (6). Based on the Boltzmann superposition principle, the stress–strain relationship is

$$\sigma = Y_f(t)^* \mathrm{d}\varepsilon, \tag{7}$$

where $Y_f(t)$ is the relaxation modulus of the material and * represents the convolution operation. And the relaxation modulus of the present multi-branch fractional Maxwell model can be expressed as

$$Y_f(t) = E_0 + \sum_{i=1}^{n} E_i f_{\alpha_i}\left(-\left(\frac{t}{\tau_i}\right)^{\alpha_i}\right), \tag{8}$$

where $f_{\alpha_i}(t)$ is the Mittag–Leffler function of the ith branch

$$f_{\alpha_i}(x) = \sum_{k=0}^{\infty} \frac{x^k}{\Gamma(1 + \alpha k)}. \tag{9}$$

It should be noted that although the Boltzmann superposition principle is only suitable to small deformation cases generally, it could be extended to large deformation cases by decomposing the time interval into very small parts in which the stresses could be superposed linearly.

2.2. Temperature effect

The relaxation time τ_i of the SMP strongly depends on temperature which is the key to the SME as well as the temperature-dependent Young's modulus. Published literature suggests that the well-established 'thermo-rheological simplicity' principle [30] effectively depicts the temperature-dependence of relaxation time

$$\tau_i = \tau_i^0 a_T(T), \tag{10}$$

where τ_i^0 is the reference relaxation time, and $a_T(T)$ is the time-temperature superposition shifting factor and can be described by the William–Lander–Ferry equation [31] above the reference temperature T_r and by the Arrhenius law [32] below T_r as

$$\begin{cases} \log a_T = -\dfrac{C_1(T - T_r)}{C_2 + T - T_r} & T \geqslant T_r \\ \ln a_T = -\dfrac{AF_c}{k_b}\left(\dfrac{1}{T} - \dfrac{1}{T_r}\right) & T < T_r \end{cases}, \tag{11}$$

where C_1, C_2, A are material constants, F_c and k_b are the configuration energy and Boltzmann constant, respectively.

2.3. Viscous flow rule

The molecular mechanism of the viscous flow is considered as overcoming the shear resistance for chain rearrangement. So the simplified isotropic uniaxial flow rule is

$$\dot{\lambda}_i^{\,v} = \frac{1}{\sqrt{3}} \lambda_i^v \dot{\gamma}^v, \tag{12}$$

where $\lambda_i^v = \varepsilon_i^v + 1$ is the extension ratio of plastic shear deformation gradient of the ith branch and $\dot{\gamma}^v$ is the viscous stretch. The Eying model [33] is able to describe the evolution of $\dot{\gamma}^v$.

$$\dot{\gamma}^v = R_y \frac{T s_y}{Q_s} \exp\left(-\frac{B}{T}\right) \sinh\left(\frac{Q_s \overline{\tau}}{T s_y}\right), \tag{13}$$

where R_y is the rate-dependent yielding factor, s_y is the yielding stress, Q_s and B are the activation parameters, and $\overline{\tau} = \sigma/\sqrt{3}$ is the equivalent shear stress. The evolution rule of s_y in the post-yielding strain softening process is

$$\dot{s}_y = h\left(1 - \frac{s_y}{s_s}\right)\dot{\gamma}^v, \quad s_y(0) = s_0, \tag{14}$$

where h is the yielding variable describing the rate of softening, s_s and s_0 are the steady and initial values of s_y, respectively. According to the experimental results, we find that the following form of R_y is effective in describing the strain rate-dependence of the yielding behaviors.

$$R_y = \begin{cases} 1 + (D_r \dot{\varepsilon})^q & \dot{\varepsilon} > \dot{\varepsilon}_q \\ 1 & \dot{\varepsilon} \leqslant \dot{\varepsilon}_q \end{cases}, \tag{15}$$

where D_r and q are the material parameters describing the strain rate-dependence, and $\dot{\varepsilon}_q$ is the quasi-static strain rate-dependent on specific experiments.

2.4. Parameter determination

The parameters involved in the relaxation modulus $Y_f(t)$ can be determined by fitting the storage modulus and loss factor curves from a single DMA temperature sweep experiment at a constant frequency. It is very efficient, and the number of branches needed is determined by the specific materials and the experimental results. The frequency-dependent storage modulus $G'(w)$, loss modulus $G''(w)$ and loss factor $\tan\delta(w)$

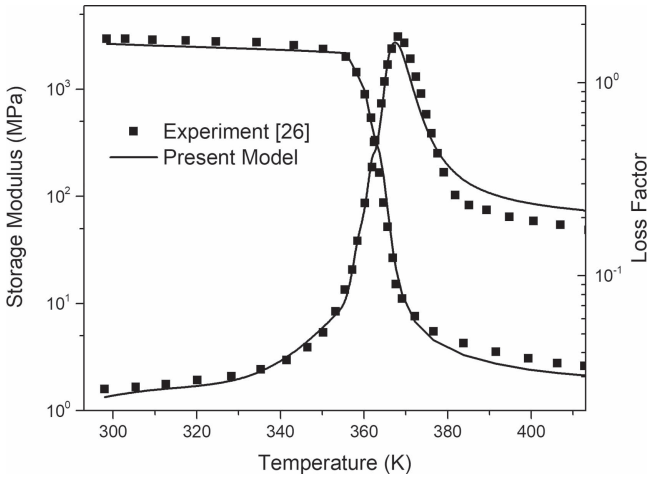

Figure 2. DMA curves and fitting results of the Veriflex-Epoxy thermosetting SMP.

are obtained by Fourier transform of equation (6).

$$G'(w) = \sum_{i=1}^{n} E_i \frac{w^{2\alpha_i}\tau_i^{2\alpha_i} + w^{\alpha_i}\tau_i^{\alpha_i}\cos(\pi\alpha_i/2)}{1 + w^{2\alpha_i}\tau_i^{2\alpha_i} + 2w^{\alpha_i}\tau_i^{\alpha_i}\cos(\pi\alpha_i/2)}, \quad (16)$$

$$G''(w) = \sum_{i=1}^{n} E_i \frac{w^{\alpha_i}\tau_i^{\alpha_i}\sin(\pi\alpha_i/2)}{1 + w^{2\alpha_i}\tau_i^{2\alpha_i} + 2w^{\alpha_i}\tau_i^{\alpha_i}\cos(\pi\alpha_i/2)}, \quad (17)$$

$$\tan\delta(w) = G''(w)/G'(w), \quad (18)$$

where w is the angular frequency. The curve fitting operations are carried out by Mathematica based on the least square principle, and the object function is,

$$f_{\mathrm{DMA}} = \sum_{j=1}^{m}\left\{\left[\frac{G'(T_j)}{G'_j} - 1\right]^2 + \left[\frac{\tan\delta(T_j)}{\tan\delta_j} - 1\right]^2\right\}, \quad (19)$$

where $T_j (j = 1 \cdots m)$ is the temperature value of the jth experimental data point, and G'_j, $\tan\delta_j$ and $G'(T_j)$, $\tan\delta(T_j)$ are the experimental data and the theoretical values at temperature T_j.

The determination of the parameters involved in the Eying model is very similar to the method developed by Qi *et al* [21] or by Westbrook *et al* [34]. Readers can refer to these two published papers for details.

3. Results and discussion

The multi-branch fractional derivative model is employed to predict the strain rate-, hold time-, and temperature-dependent cyclic behaviors of two different kinds of amorphous SMPs subjected to cyclic tension loading at high temperatures and low temperatures, respectively. And the model is implemented by Mathematica.

3.1. The Veriflex-Epoxy thermosetting SMP

Yu *et al* [26] carried out the DMA experiments at a frequency of 1 Hz with 0.1% strain amplitude while the temperature ranges from 413 to 298 K at a heating/cooling rate of 2 K min^{-1} by a DMA tester (Model Q800, TA Instruments, New Castle, DE, USA). The fitting results are shown in figure 2 and four branches are adopted here. Compared to the existing general Maxwell model of 18 branches by Yu *et al* [26], the present model reduces 37 parameters to 17, which greatly improves the calculating efficiency. Table 1 presents the parameters involved in this case.

Table 1. Parameters for the Veriflex-Epoxy thermosetting SMP.

E_0, $E_1 \sim E_4$(MPa)		$\tau_1^0 \sim \tau_4^0$(s)		$\alpha_1 \sim \alpha_4$
0.6, 280.3, 1102.0, 755.1, 905.7		7.0×10^5, 2.98, 6480.4, 3.4×10^{-5}		0.84, 0.57, 0.74, 0.18
C_1, C_2(−,K)	AF_c/k_b(K)	T_r(K)	s_0, s_s(MPa)	Q_s(K)
13.2, 7.5	−18 736	357	70, 35	2800
B(K)	D_r(s)	q	$\dot{\varepsilon}_q$(s^{-1})	h(MPa)
4295.4	1.04×10^4	0.94	10^{-4}	400

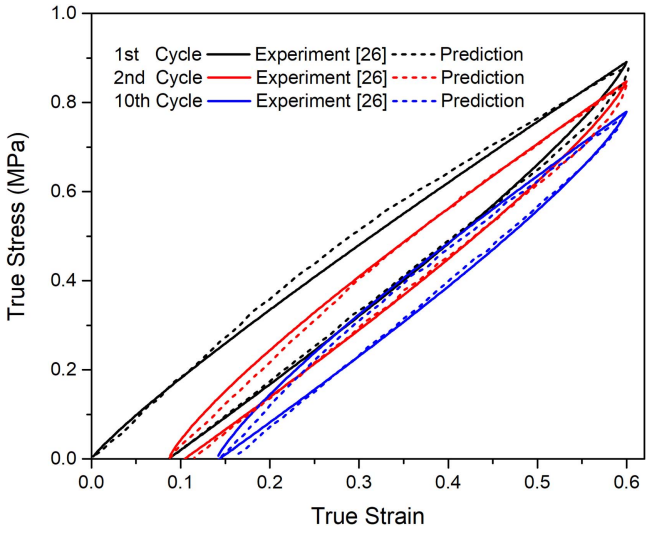

Figure 3. Stress–strain curves (1st, 2nd, 10th) in the cyclic tension at 393 K.

Cyclic tension tests were also performed on the DMA machine. The test temperature was 393 K, the loading/unloading strain rate was 2% s^{-1} in each cycle. And the samples were firstly stretched to a target strain of 60% engineering strain, then unloaded till the stress decreased to zero, and followed by the next cycle immediately. Figure 3 shows the prediction of the stress–strain behaviors in the 10 cycles at 393 K by the multi-branch fractional derivative model and its comparison with the experimental results. For the sake of clarity, only the results of the 1st, 2nd and 10th cycles are plot. It is obvious that the present model captures the cyclic behaviors at the high temperature accurately. And the stress–strain curves show the ratchet phenomenon which could be observed in many polymers subjected to cyclic loadings.

Figure 4 shows the evolution of two specific parameters versus cycle numbers, where the stress before unloading is the largest stress value in each cycle and the residual strain ratio is defined as the ratio of the residual strain at each cycle to the maximum strain, i.e., $R_{rs} = \varepsilon_r/\varepsilon_{\mathrm{M}}$. The discrepancy between

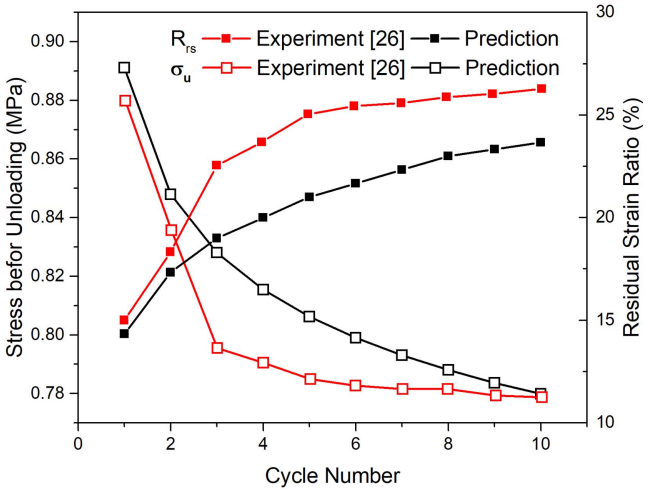

Figure 4. Stresses before unloading and residual strain ratios versus cycle numbers.

the predictions and experimental results is very small (≈0.04 MPa for σ_u and ≈4% for R_{rs}). And it is shown that the largest stress decreases gradually, while the residual strain ratio increases from 15% to 25% as the number of cycles increases. The stress–strain curves in figure 3 indicate quasi-linear properties at the specific temperature, and the residual strain accumulated in the first cycle is much bigger than the rest cycles, but the decrease of the maximum stress in each cycle is almost the same. The relaxation modulus as a function of time decreases slower and slower as time increases, which is believed to be the key to the observed phenomena.

Yu *et al* did not carry out cyclic loading experiments at low temperatures, but McClung *et al* [35] did several uniaxial tension experiments for the same material. Figures 5(a)–(c) show the comparisons between the predictions and the experimental results at the strain rates of 10^{-4}, 10^{-3} and 10^{-2}, respectively. It is obvious that both the yielding stress and the yielding strain decrease as the strain rate increases. And the present model is able to capture the influence of the strain rate, as well as the yielding and post-yielding behaviors of the SMP. The cyclic performance at low temperatures is discussed in the following section.

3.2. The polyurethane SMP

The DMA experiments of the specific material were conducted by Pieczyska *et al* [36] in a single-frequency of 1 Hz scanning mode at 2 K min^{-1} from 148 to 443 K. The temperature range is extremely large in their experiments. But the thermomechanical behaviors of the material at extremely low or high temperatures are not considered in the paper. On the one hand, it is not common in the engineering. On the other hand, the glass transition temperature equals 318 K (45 °C), hence the material is able to accomplish its SMEs from 273 to 373 K. The fitting results for DMA experiments are shown in figure 6. Three branches are used in this case. It is worth mentioning that the number of branches is determined by the specific material, and usually three branches of 14 parameters are enough.

Pieczyska *et al* [27] conducted the cyclic tension experiments for the polyurethane SMP at the room temperature of 295 K and at the strain rates of 10^{-2}, 10^{-1} and 10^{0}, respectively. The material is rigid at low temperatures. So very different behaviors are observed in the experiments, and figures 7(a)–(c) show the comparisons of the stress–strain curves between the prediction of the present model and the experimental results. The maximum strain is much small in this case, but the strain rates are much large. So the present model captures the rate-dependent yielding and post-yielding behaviors accurately, but only qualitatively describes the ratchet phenomenon of the rest cycles. It should be noted that, for example, in the case of 10° s^{-1} strain rate, the first cycle is accomplished in about 0.08 s while the rest cycles are accomplished in less than 0.01 s. It is difficult to record enough data accurately, so the experimental error should not be ignored. In general, the present model is able to well describe the thermomechanical behaviors of SMPs subjected to cyclic tension loadings at temperatures above or below the glass transition temperature.

3.3. Parameter study

The cyclic mechanical properties of SMPs are influenced by many factors which affect the performance of the materials in engineering. So several key factors such as strain rates, temperatures, hold times and cycle numbers are studied detailedly in this section to provide helpful guidelines for engineering. The material discussed in the section is the polyurethane SMP.

The effect of the temperature is the most significant. Figure 8 plots residual strain ratios R_{rs} versus cycle numbers at different temperatures ranging from 353 K to 293 K, the imposed maximum strain is 12%, and the strain rate is 0.1 s^{-1}. The residual strain accumulates cycle by cycle at any temperature. But when the temperature is higher or lower enough than the glass transition temperature, the residual strain tends to be stable after 10 cycles. At the temperature very close to T_g, the residual strain ratio increases from 30% to 60% in the first 10 cycles and then increases to 80%. Obviously, the temperature is of great influence on the residual strain ratio, R_{rs} is less than 20% at high temperatures, while the imposed strain rarely recovers at 293 K. These phenomena are due to the particular properties of SMPs. It is believed that the residual strain ratio is determined by the temperature-dependent elastic properties of the materials. At temperatures above T_g, the materials behave hyperelastic and can recover most of the imposed deformation. As temperature decreases, the viscoplasticity gradually dominates, and the modulus significantly increases several orders of magnitudes. As shown in figure 7, plastic flow occurs when the strain increases to 3% at 295 K. The plastic strain is unable to recover spontaneously at the same temperature resulting to a much larger residual strain ratio. And if the materials are heated freely, the strain can fully recover. That is because the molecular chain mobility increases significantly above the glass transition temperature, so the chains spontaneously recover to equilibrium state. As figure 9 shows, in order to

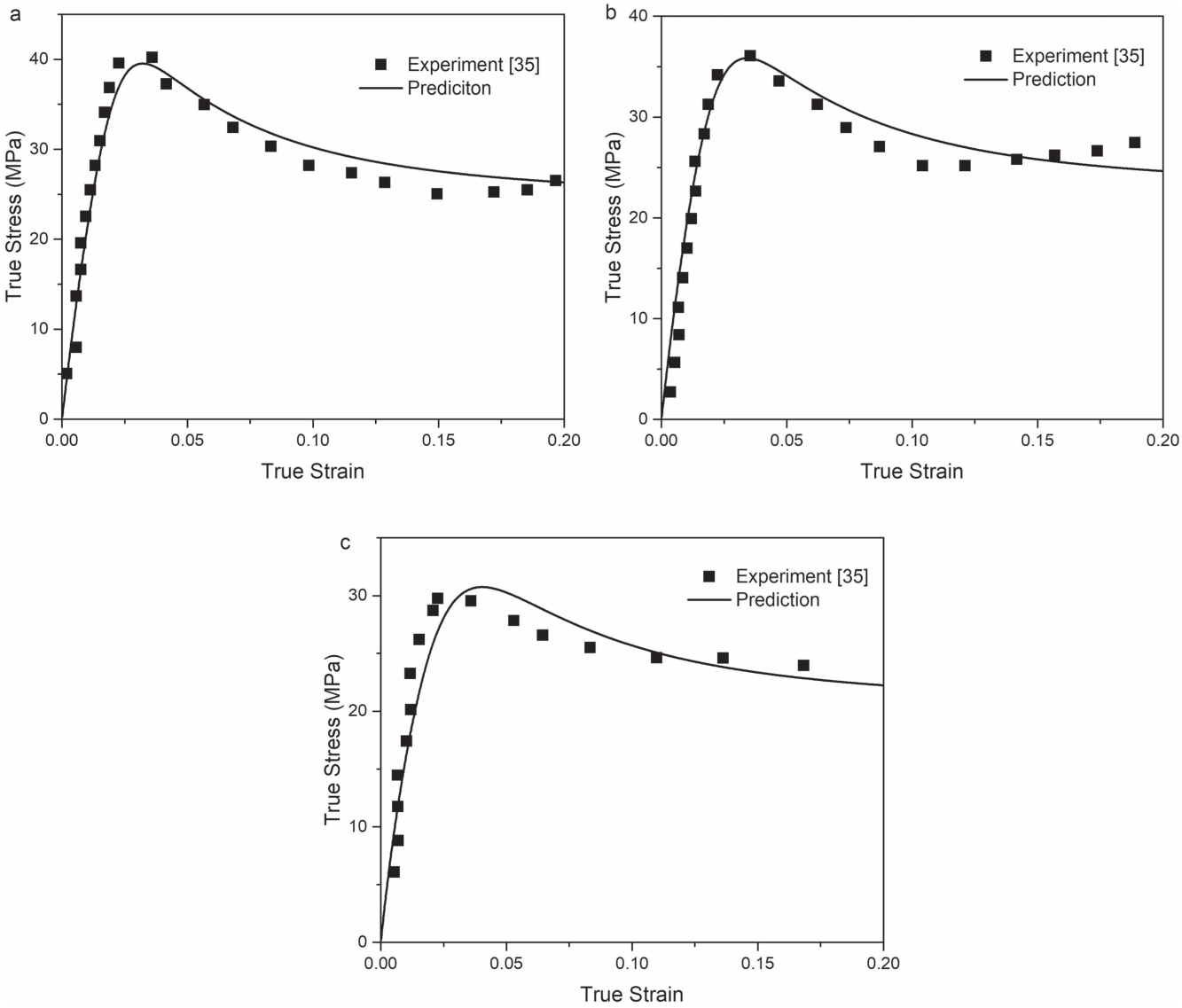

Figure 5. Stress–strain curves for uniaxial tension experiments at 333 K at different strain rates of (a) 10^{-4} (b) 10^{-3} and (c) 10^{-2}.

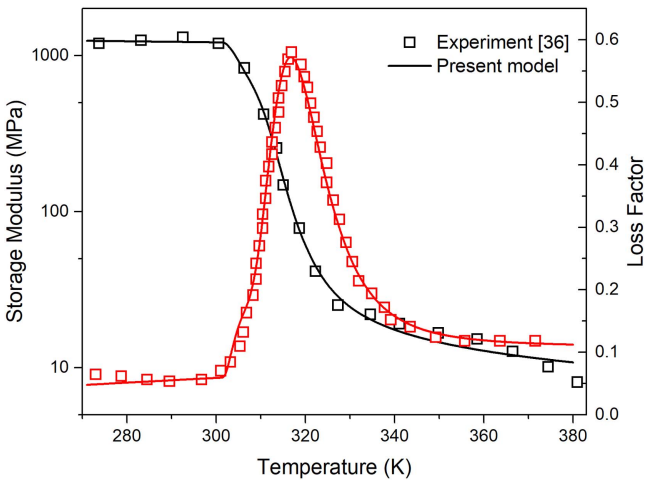

Figure 6. DMA curves and fitting results for the polyurethane SMP.

reduce the residual strain ratio, raising temperature is effective, and the effectiveness decreases when the temperature is high enough.

Figure 10 shows the predictions of the stress–strain curves at different strain rates under cyclic tension conditions at 313 K. The temperature is a little lower than T_g, at which the impact of the strain rate is more obvious. Due to the decease of the relaxation effect, the stress increases significantly with increasing strain rate. The influence of the strain rate on the residual strain ratio is shown in figure 11. The temperature is also 313 K in each case. In general, the residual strain ratio finally increases to 95% regardless of the strain rate. It indicates that the residual strain is determined by the elasticity and plasticity of the material. As for SMPs, the temperature is the key factor to the elastic and plastic properties, so the residual strain ratios tend to be the same at the same temperature. However, in the first several cycles, the influence of the strain rate is also noticeable. The residual strain ratio decreases about 20% in the first cycle at the strain

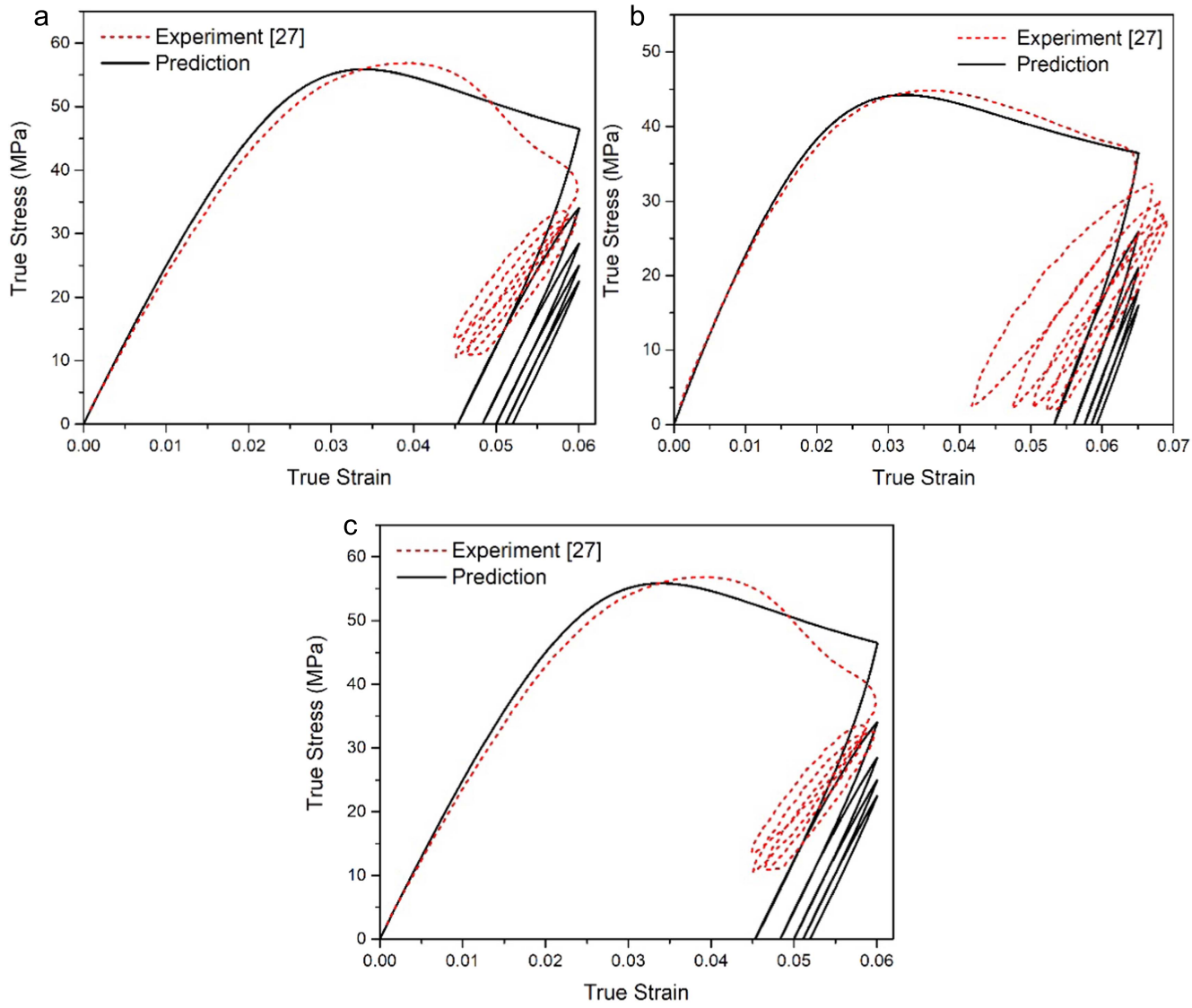

Figure 7. Stress–strain curves for cyclic tension experiments at 295 K at different strain rates of (a) 10^{-2} (b) 10^{-1} and (c)10^{0}.

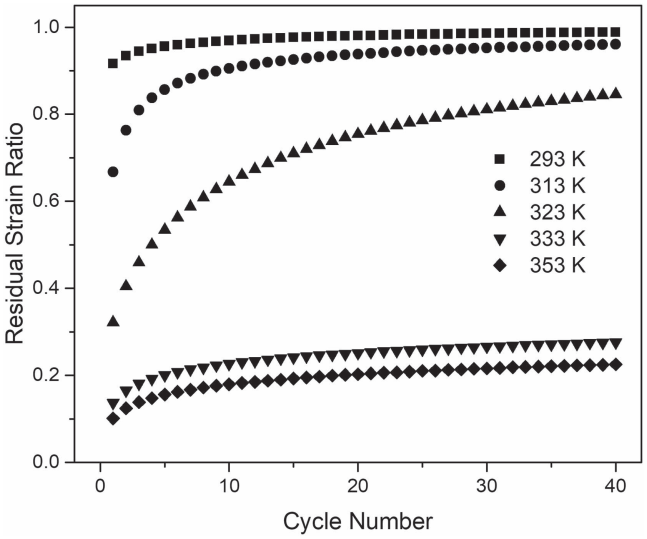

Figure 8. Residual strain ratios versus cycle numbers at different temperatures.

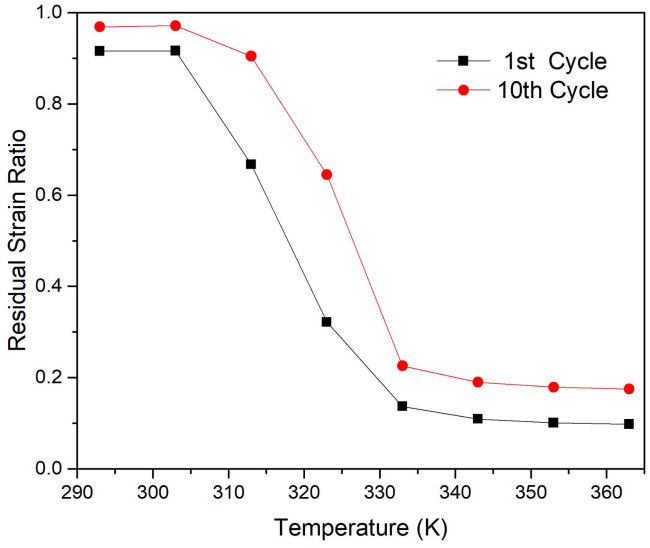

Figure 9. Residual strain ratios versus temperatures in the 1st and 10th cycles.

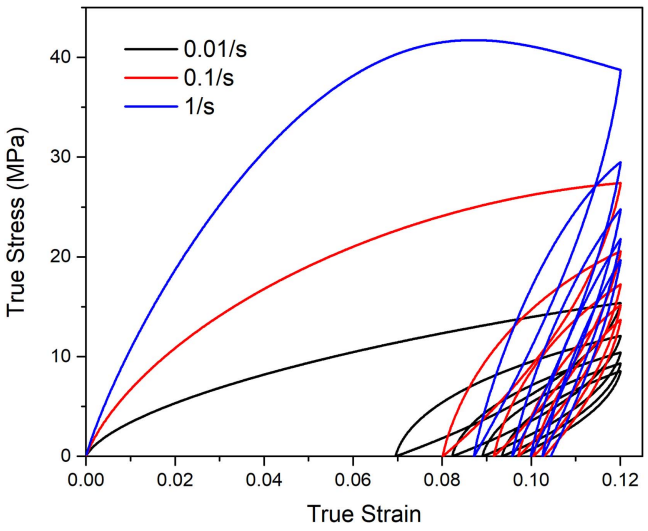

Figure 10. Stress–strain curves at different strain rates under cyclic tension conditions.

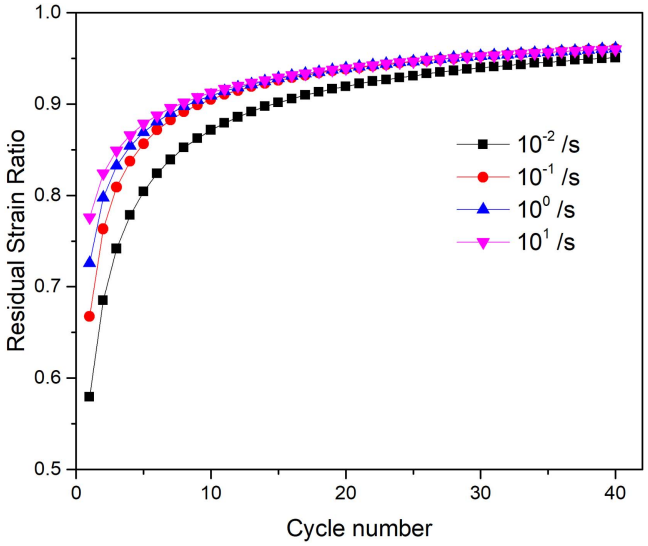

Figure 11. Residual strain ratios versus cycle numbers at different strain rates.

rate of $10^{-2}\,s^{-1}$, and increases slower cycle by cycle. It may be effective to slow down, but the time cost dramatically increases correspondingly. So it depends on the application cases in engineering.

Another important impact factor is the hold time, which means that the material is held for a few seconds after each cycle before the next one. Figure 12 provides a visualized image for the influence of the hold time t_{hold}. The temperature is 313 K and the strain rate is $0.1\,s^{-1}$. In the first cycle, the residual strain recovers from 8% to 4.8% during the hold time. Nevertheless, the unloading process is almost the same in the next cycle. It indicates that the residual strain recovers during holding because of the relaxation mechanisms, but the initial residual strain is determined by the elastic properties of SMPs which are determined by the temperature. Therefore, we investigate the influence of hold times versus cycle numbers at two temperatures. The results are shown in

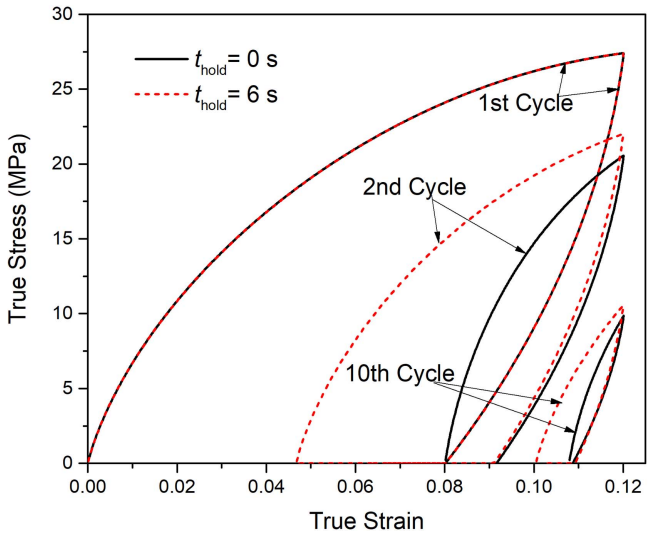

Figure 12. Stress–strain curves for different hold times under cyclic tension conditions.

figures 13(a) and (b), the temperatures are 353 and 313 K, and the strain rate is $0.1\,s^{-1}$. The difference is obvious at the two different temperatures. In the 40th cycle, the residual strain ratio decreases nearly 20% with a 6 s hold time at 353 K, while the ratios are almost the same at 313 K. It is because that the plasticity of SMPs is small at high temperatures, and the materials are able to recover their strain gradually. In the glass transition region, the plasticity accumulates and then dominates gradually. So the influence of the hold time decreases gradually. In addition, it should be noted that, although the residual strain ratio decreases from 20% to 6% with a 6 s hold time, the time of each cycle increases from 1 to 7 s. So it is believed that 0.6 s or 1 s may be the most efficient option to enhance the performance of the material in engineering.

4. Conclusions

In the paper, we thoroughly investigate the thermomechanical behaviors of amorphous SMPs subjected to cyclic tension loadings under various conditions. The multi-branch fractional derivative model is employed due to its simplicity, accurateness and adaptability. A rate-dependent yielding factor is proposed to extend the Eying model to capture the strain rate-dependent yielding and post-yielding behaviors of SMPs. Through the comparisons between the predictions by the present model and the experimental results, the validation of the model is verified. In general, the following conclusions can be drawn from the study:

(1) The model is valid for the strain rate-, hold time-, and temperature-dependent cyclic stress–strain response of amorphous SMPs such as Veriflex-Epoxy thermosetting SMPs and polyurethane SMPs. And the model is able to predict the cyclic behaviors of the materials under various conditions.

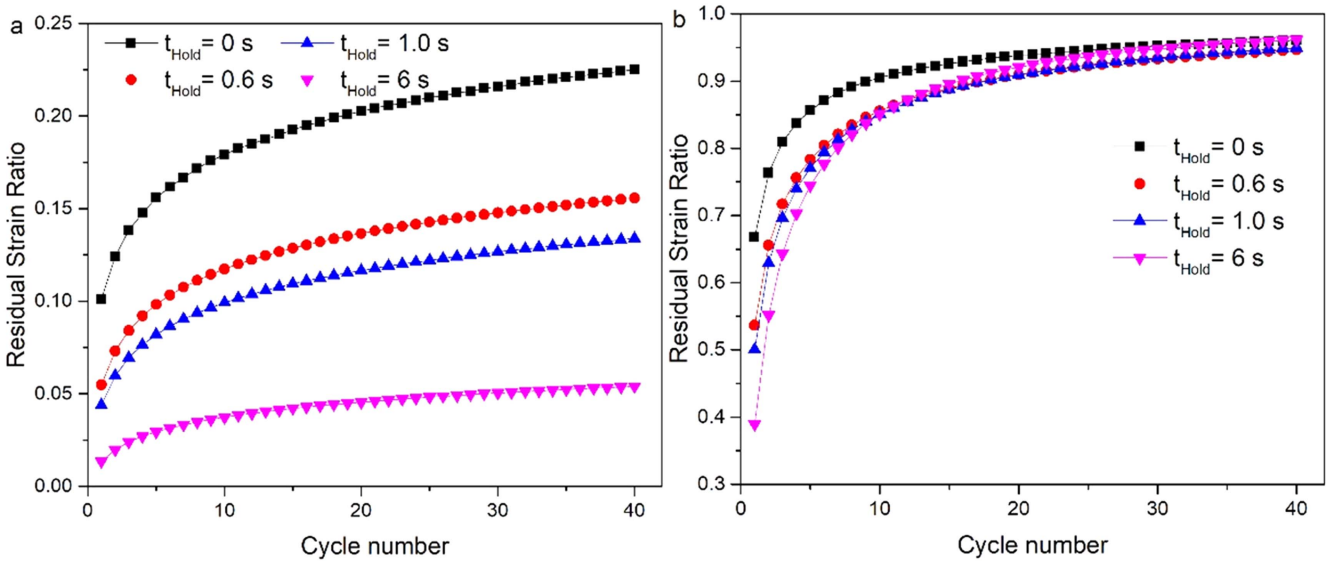

Figure 13. Residual strain ratios versus cycle numbers for different hold times at (a) 353 and (b) 313 K.

(2) Temperature is the key factor to the cyclic performance of SMPs. Increasing the temperature above the glass transition temperature can significantly reduce the residual strain ratio and enhance the cyclic properties of the materials.
(3) Strain rates influence the cyclic behaviors of SMPs in the first few cycles. The stress response as well as the residual strain ratio increases at faster strain rates. Reducing strain rates is effective to enhance the recovery of the materials at first, but the residual strain ratios increase to the same value finally. Moreover, slowing down increases the time cost.
(4) The residual strain ratio can be reduced with a hold time at the end of each cycle. The enhancement of hold time to the cyclic behaviors at temperatures around the glass transition temperature is significant at the beginning but disappears gradually as the number of cycles increases. However, the influence at high temperatures can be maintained all through.
(5) It is always effective to enhance the cyclic performance of SMPs by increasing the temperature, slowing down the strain rate or adding the hold time. But the most efficient option of proper values of the temperature, strain rate and hold time depends on the specifitc cases in engineering. The present study provides helpful guidelines for determining the proper values.

Acknowledgments

This work is supported by the National Natural Science Foundation of China (11572153), the Natural Science Foundation of Jiangsu Province of China (BK20151467, BK20170759), the Postgraduate Research & Practice Innovation Program of Jiangsu Province (KYCX17_0231), the Fundation of Graduate Innovation Center in NUAA (kfjj20170115) and a project funded by the Priority Academic Program Development of Jiangsu Higher Education Institutions (PAPD).

ORCID iDs

Hao Zeng https://orcid.org/0000-0002-1862-7878
Jinsong Leng https://orcid.org/0000-0001-5098-9871
Huiyu Sun https://orcid.org/0000-0001-8500-960X

References

[1] Behl M and Lendlein A 2007 Shape-memory polymers *Mater. Today* **10** 20–8
[2] Liu C, Qin H and Mather P T 2007 Review of progress in shape-memory polymers *J. Mater. Chem.* **17** 1543
[3] Lendlein A, Jiang H, Jünger O and Langer R 2005 Light-induced shape-memory polymers *Nature* **434** 879–82
[4] Long K N, Scott T F, Jerry Q H, Bowman C N and Dunn M L 2009 Photomechanics of light-activated polymers *J. Mech. Phys. Solids* **57** 1103–21
[5] Buckley P R, McKinley G H, Wilson T S, Small W IV, Benett W J, Bearinger J, McElfresh M W and Maitland D J 2006 Inductively-heated shape memory polymer for the magnetic actuation of medical devices *IEEE Trans. Biomed. Eng.* **53** 2075–83
[6] Conti S, Lenz M and Rumpf M 2007 Modeling and simulation of magnetic-shape-memory polymer composites *J. Mech. Phys. Solids* **55** 1462–86
[7] Chan B Q Y, Low Z W K, Heng S J W, Chan S Y, Owh C and Loh X J 2016 Recent advances in shape memory soft materials for biomedical applications *ACS Appl. Mater. Interfaces* **8** 10070–87
[8] Liu Y, Du H, Liu L and Leng J 2014 Shape memory polymers and their composites in aerospace applications: a review *Smart Mater. Struct.* **23** 023001
[9] Tobushi H, Hara H, Yamada E and Hayashi S 1996 Thermomechanical properties in a thin film of shape memory polymer of polyurethane series *Smart Mater. Struct.* **5** 483–91

[10] Tobushi H, Hashimoto T, Hayashi S and Yamada E 1997 Thermomechanical constitutive modeling in shape memory polymer of polyurethane Series *J. Intell. Mater. Syst. Struct.* **8** 711–8
[11] Chen J, Liu L, Liu Y and Leng J 2014 Thermoviscoelastic shape memory behavior for epoxy-shape memory polymer *Smart Mater. Struct.* **23** 55025
[12] Chen Y C and Lagoudas D C 2008 A constitutive theory for shape memory polymers: I. Large deformations *J. Mech. Phys. Solids* **56** 1752–65
[13] Chen Y C and Lagoudas D C 2008 A constitutive theory for shape memory polymers: II. A linearized model for small deformations *J. Mech. Phys. Solids* **56** 1766–78
[14] Nguyen T D, Jerry Q H, Castro F and Long K N 2008 A thermoviscoelastic model for amorphous shape memory polymers: Incorporating structural and stress relaxation *J. Mech. Phys. Solids* **56** 2792–814
[15] Gu J, Sun H and Fang C 2015 A finite deformation constitutive model for thermally activated amorphous shape memory polymers *J. Intell. Mater. Syst. Struct.* **26** 1530–8
[16] Diani J, Gilormini P, Frédy C and Rousseau I 2011 Predicting thermal shape memory of crosslinked polymer networks from linear viscoelasticity *Int. J. Solids Struct.* **49** 793–9
[17] Azzawi W A, Epaarachchi J A, Islam M and Leng J 2017 Implementation of a finite element analysis procedure for structural analysis of shape memory behaviour of fibre reinforced shape memory polymer composites *Smart Mater. Struct.* **26** 125002
[18] Xiao R, Choi J, Lakhera N, Yakacki C M, Frick C P and Nguyen T D 2013 Modeling the glass transition of amorphous networks for shape-memory behavior *J. Mech. Phys. Solids* **61** 1612–35
[19] Liu Y, Gall K, Dunn M L, Greenberg A R and Diani J 2006 Thermomechanics of shape memory polymers: uniaxial experiments and constitutive modeling *Int. J. Plast.* **22** 279–313
[20] Baghani M, Naghdabadi R and Arghavani J 2013 A large deformation framework for shape memory polymers: constitutive modeling and finite element implementation *J. Intell. Mater. Syst. Struct.* **24** 21–32
[21] Qi H J, Nguyen T D, Castro F, Yakacki C M and Shandas R 2008 Finite deformation thermo-mechanical behavior of thermally induced shape memory polymers *J. Mech. Phys. Solids* **56** 1730–51
[22] Boatti E, Scalet G and Auricchio F 2016 A three-dimensional finite-strain phenomenological model for shape-memory polymers: formulation, numerical simulations, and comparison with experimental data *Int. J. Plast.* **83** 153–77
[23] Park H, Harrison P, Guo Z, Lee M G and Yu W R 2016 Three-dimensional constitutive model for shape memory polymers using multiplicative decomposition of the deformation gradient and shape memory strains *Mech. Mater.* **93** 43–62
[24] Guo X, Liu L, Liu Y, Zhou B and Leng J 2014 Constitutive model for a stress- and thermal-induced phase transition in a shape memory polymer *Smart Mater. Struct.* **23**
[25] Li Y, He Y and Liu Z 2017 A viscoelastic constitutive model for shape memory polymers based on multiplicative decompositions of the deformation gradient *Int. J. Plast.* **91** 300–17
[26] Yu K, Li H, McClung A J W, Tandon G P, Baur J W and Qi H J 2016 Cyclic behaviors of amorphous shape memory polymers *Soft Matter* **12** 3234–45
[27] Pieczyska E A, Staszczak M, Kowalczyk-Gajewska K, Maj M, Golasiński K, Golba S, Tobushi H and Hayashi S 2017 Experimental and numerical investigation of yielding phenomena in a shape memory polymer subjected to cyclic tension at various strain rates *Polym. Test.* **60** 333–42
[28] Fang C, Leng J, Sun H and Gu J 2018 A multi-branch thermoviscoelastic model based on fractional derivatives for free recovery behaviors of shape memory polymers *Mech. Mater.* **120** 34–42
[29] Koeller R C 1984 Applications of fractional calculus to the theory of viscoelasticity *J. Appl. Mech.* **51** 299
[30] Rubinstein M and Colby R H 2003 *Polymer Physics* (New York: Oxford University Press)
[31] Williams M L, Landel R F and Ferry J D 1955 The Temperature dependence of relaxation mechanisms in amorphous polymers and other glass-forming liquids *J. Am. Chem. Soc.* **77** 3701–7
[32] Di M E A and Yang A J M 1997 Configurational entropy approach to the kinetics of glasses *J. Res. Natl Inst. Stand. Technol.* **102** 135–57
[33] Eyring H 1936 Viscosity, plasticity, and diffusion as examples of absolute reaction rates *J. Chem. Phys.* **4** 283–91
[34] Westbrook K K, Kao P H, Castro F, Ding Y and Jerry Q H 2011 A 3D finite deformation constitutive model for amorphous shape memory polymers: a multi-branch modeling approach for nonequilibrium relaxation processes *Mech. Mater.* **43** 853–69
[35] McClung A J W, Tandon G P and Baur J W 2012 Strain rate- and temperature-dependent tensile properties of an epoxy-based, thermosetting, shape memory polymer (Veriflex-E) *Mech. Time-Dependent Mater.* **16** 205–21
[36] Pieczyska E A, Staszczak M, Maj M, Kowalczyk-Gajewska K, Golasiński K, Cristea M, Tobushi H and Hayashi S 2016 Investigation of thermomechanical couplings, strain localization and shape memory properties in a shape memory polymer subjected to loading at various strain rates *Smart Mater. Struct.* **25** 085002